Contribution from the Department of Chemistry,
University of Houston, Houston, Texas 77204-5641

Molecular Structure and Chemical and Electrochemical Reactivity of $Co_2(dpb)_4$ and $Rh_2(dpb)_4$ (dpb = *N,N'*-Diphenylbenzamidinate)

L.-P. He, C.-L. Yao, M. Naris, J. C. Lee, J. D. Korp, and J. L. Bear*

Received March 5, 1991

The reaction of bis(4-cyclohexylbutyrato)cobalt(II), $Co(C_{10}H_{17}O_2)_2$, with the lithium salt of *N,N'*-diphenylbenzamidine in tetrahydrofuran results in the formation of tetrakis(μ-*N,N'*-diphenylbenzamidinato)dicobalt(II), $Co_2(dpb)_4$ (**1**). The crystal and molecular structure of **1** has been determined by X-ray diffraction. The complex crystallizes in space group $C2/c$ with a = 24.189 (8) Å, b = 12.201 (4) Å, c = 24.283 (7) Å, β = 115.34 (2)°, and Z = 4. The Co–Co separation is 2.302 Å, and the average Co–N bond distance is 1.942 Å. The mean N–Co–Co–N torsion angle is 18.4°. The crystal and molecular structures of $Rh_2(dpb)_4$ (**2**) and $Rh_2(dpb)_4(CO)$ (**3**) have also been determined. Compound **2** crystallizes in space group $P4/n$ with a = 17.467 (4) Å, c = 12.119 (2) Å, and Z = 2. The Rh–Rh bond distance is 2.389 (1) Å, and the average Rh–N separation is 2.050 (2) Å. The N–Rh–Rh–N torsion angle is 17.3°. $Rh_2(dpb)_4(CO)$ crystallizes in space group $P4/ncc$ with a = 17.473 (4) Å, c = 23.762 (4) Å, and Z = 4. Formation of the CO adduct increases the Rh–Rh bond distance to 2.435 (1) Å. R values for the refinements of **1**–**3** were 0.046, 0.040, and 0.049. $[Co_2(dpb)_4]^+$ gives a complicated ESR spectrum in frozen solution (122 K) with g_3 at 1.98 split into 15 equally spaced lines (A_3 = 98.6 × 10^{-4} cm^{-1}) by the two ^{59}Co ions (I = $^7/_2$, 100% natural abundance). The ESR spectrum of the radical anion complex, $[Co_2(dpb)_4]^-$, gives an axial signal with $g_\parallel$ split into 15 lines ($A_\parallel$ = 39.0 × 10^{-4} cm^{-1}). Nuclear coupling is also observed in $g_\perp$ ($A_\perp$ = 16.8 × 10^{-4} cm^{-1}). The hyperfine splitting observed in g_3 and $g_\parallel$ for the two complexes is consistent with the odd-electron spin density being equally distributed over the two cobalt centers. Visible spectra, redox reactions, and ESR spectra of the dicobalt and dirhodium complexes studied are quite similar. Unlike the dirhodium complexes, the cobalt dimer shows little tendency to form axial adducts.

Introduction

The $3d^7$ cobalt(II) ion displays little tendency to form complexes with a strong M–M bond. As a result, only a few complexes containing the Co_2^{4+} unit have been reported and little is known about their electrochemical properties, oxidation-state stabilities, spectroscopic properties, and chemical reactivity. This is in sharp contrast to the voluminous and expanding literature on $4d^7$ dinuclear rhodium(II) compounds. Dirhodium(II) tetracarboxylates have been studied extensively, and there are several review articles on the subject.[1,2] All of the dirhodium complexes have a strong metal–metal bond and are diamagnetic. Several dicobalt(II) carboxylates have also been reported;[3-6] however, only $Co_2(OOCPh)_4$(quinoline) has been structurally characterized. The molecule has a long Co–Co separation of 2.832 Å and magnetic properties consistent with antiferromagnetic exchange through the bridge.[5] Even with the forced proximity of the two Co(II) ions, there appears to be little metal–metal interaction in carboxylate-bridged complexes.

The synthesis and molecular structure of tetrakis(μ-*N,N'*-diphenyltriazinato)dicobalt(II), $Co_2(triaz)_4$, have been recently reported,[7] as well as its electronic structure investigated by means of SCF-Xα-SW calculations.[8] The electronic spectra and electrochemical properties of $Co_2(triaz)_4$ were not reported. The molecule has a short Co–Co separation of 2.265 Å, indicating a strong Co–Co interaction. Apparently, ligation by the strongly basic nitrogen donors of the *N,N'*-diphenyltriazinate ions stabilize the Co(II)–Co(II) bond. It appeared to us that the structurally similar complex $Co_2(dpb)_4$ (compound **1**) (dpb = *N,N'*-diphenylbenzamidinate ion) could be synthesized and its chemical and electrochemical properties compared to those of the dirhodium complex, $Rh_2(dpb)_4$ (compound **2**.).[9] We were successful in synthesizing **1** and herein report the molecular structure, chemical and electrochemical reactivity, and spectroscopic properties of the complex. The molecular structure of $Rh_2(dpb)_4(CO)$ (compound **3**) and a more detailed electrochemical and spectroscopic investigation of **2** and its singly oxidized and reduced state are also reported for comparison.

Experimental Section

Chemicals. All solvents were purified by standard literature methods.[10] Bis(4-cyclohexylbutyrato)cobalt(II) was purchased from Eastman Kodak Co. and used without further purification. Tetrabutylammonium perchlorate (TBAP) was twice recrystallized from ethanol.

Preparation of $Co_2(dpb)_4$. A 50-mL tetrahydrofuran solution containing 0.80 g (2.0 mmol) of bis(4-cyclohexylbutyrato)cobalt(II), $Co(C_{10}H_{17}O_2)_2$, and 1.11 g (4.0 mmol) of lithium *N,N'*-diphenylbenzamidinate, $Li^+(dpb)^-$, was refluxed under argon with stirring for 24 h. Lithium *N,N'*-diphenylbenzamidinate was freshly prepared by the reaction of butyllithium with *N,N'*-diphenylbenzamidine in tetrahydrofuran. The color of the solution changed from dark purple to brown during the reaction. The solution was filtered and the solvent removed using a rotary evaporator. The brown solid was then purified three times on a silica gel column with 1:1 CH_2Cl_2/hexane as the eluent. The yield after purification was 41%. The FAB mass spectrum of the complex gave major mass peaks at m/z 1202 ($[Co_2(dpb)_4]^+$), 931 ($[Co_2(dpb)_3]^+$), and 660 ($[Co_2(dpb)_2]^+$). Elemental analysis was performed by Texas Analytical Laboratories, Inc. Anal. Calcd for $C_{76}H_{60}N_8Co_2$: C, 75.86; H, 5.02; N, 9.31; Co, 9.79. Found: C, 75.11; H, 5.02; N, 9.13; Co, 9.75. The complex slowly decomposes in the solid state and in solution over a period of several days, producing a highly insoluble material. The complex crystallizes from a CH_2Cl_2/hexane solution as dark reddish brown crystals upon slow evaporation.

Synthesis of $Rh_2(dpb)_4$. Compound **2** was synthesized by a previously reported procedure.[9]

Synthesis of $Rh_2(dpb)_4(CO)$. The CO adduct of **2** was obtained by passing CO gas through a CH_2Cl_2 solution of the complex at room temperature. The color of the solution changed from brownish gold to blood red after a few minutes. Slow evaporation of the solvent resulted in the formation of dark red crystals. The complex was recrystallized from acetone to give small burgundy-colored crystals of $Rh_2(dpb)_4(CO)$ suitable for X-ray structure determination.

Instrumentation. ESR spectra were measured on a Bruker Model 100D ESR spectrometer. Cyclic voltammetric measurements were carried out on an IBM EC 225 voltammetric analyzer utilizing a three-electrode configuration. The working electrode consisted of a platinum button with a surface area of 0.19 mm^2. A saturated calomel electrode (SCE) was used as the reference electrode. For controlled-

(1) Boyar, E. B.; Robinson, S. D. *Coord. Chem. Rev.* **1983**, *50*, 109.
(2) Felthouse, T. R. *Progress in Inorganic Chemistry*; John Wiley and Sons: New York, 1982; Vol. 29, p 73.
(3) Boyd, P. D.; Gerloch, M.; Harding, J. H.; Woolley, R. G. *Proc. R. Soc. London A* **1978**, *360*, 161.
(4) Little, R.; Staughn, B. P.; Thornton, P. *J. Chem. Soc., Dalton Trans.* **1986**, 2211.
(5) Catterick, J.; Hursthouse, M. B.; Thornton, P.; Welch, A. J. *J. Chem. Soc., Dalton Trans.* **1977**, 223.
(6) Catterick, J.; Hursthouse, M. B.; Thornton, P.; Welch, A. J. *J. Chem. Soc., Chem. Commun.* **1973**, 52.
(7) Cotton, F. A.; Poli, R. *Inorg. Chem.* **1987**, *26*, 3652.
(8) Cotton, F. A.; Feng, X. *Inorg. Chem.* **1989**, *28*, 1180.
(9) Le, J. C.; Chavan, M. Y.; Chau, L. K.; Bear, J. L.; Kadish, K. M. *J. Am. Chem. Soc.* **1985**, *107*, 7195.
(10) Perrin, D. D.; Armrego, W. L. F.; Perrin, D. R. *Purification of Laboratory Chemicals*; Pergamon: New York, 1980.

0020-1669/92/1331-0620$03.00/0

Table I. Data Collection and Processing Parameters

	$Co_2(dpb)_4$	$Rh_2(dpb)_4$	$Rh_2(dpb)_4(CO)$
space group	$C2/c$, monoclinic	$P4/n$, tetragonal	$P4/ncc$, tetragonal
cell constants			
a, Å	24.189 (8)	17.467 (4)	17.473 (4)
b, Å	12.201 (4)		
c, Å	24.283 (7)	12.119 (2)	23.762 (4)
β, deg	115.34 (2)		
V, Å^3	6477	3698	7254
mf	$C_{76}H_{60}N_8Co_2$	$C_{76}H_{60}N_8Rh_2 \cdot 1.2C_2H_6O$	$C_{77}H_{60}N_8ORh_2 \cdot 8H_2O$
fw	1203.30	1346.5	1463
Z	4	2	4
ρ(calcd), g cm^{-3}	1.23	1.21	1.34
μ, cm^{-1}	5.57	4.80	5.05
λ(Mo Kα), Å	0.71073	0.71073	0.71073
$R(F_o)^a$	0.046	0.040	0.049
$R_w(F_o)^a$	0.035	0.048	0.053

[a] Agreement factors defined as $R = \sum||F_o| - |F_c||/\sum|F_o|$ and $R_w = [\sum w(|F_o| - |F_c|)^2/\sum|F_o|^2]^{1/2}$.

potential coulometry, a BAS Model SP-2 synthetic potentiostat was used. A Perkin-Elmer Model 330 spectrometer was used to record electronic absorption spectra.

X-ray Data Collection and Processing for $Co_2(dpb)_4$. Dark reddish brown crystals suitable for X-ray diffraction were grown by slow evaporation of a CH_2Cl_2/hexane solution. Two different types of crystals were formed simultaneously during the crystallization of $Co_2(dpb)_4$. Although it is not possible to tell them apart by eye when fresh from solution, within a few hours of exposure to air one type completely disintegrates to a brown powder while the other type remains nicely crystalline. The volatile sample was determined to consist of the tetrabridged dimer, plus massively disordered solvent which could not be precisely identified but is most likely methylene chloride. The space group is $C2/c$, with a = 25.327 (6) Å, b = 12.107 (3) Å, c = 24.800 (6) Å, β = 115.22 (2)°, and Z = 4. Data collection on this sample had to be prematurely aborted due to movement of the crystal in the solvent-filled capillary, and since no other examples of this crystal survived, the problem was abandoned. The stable crystal form was then examined, and a dark reddish brown fragment having approximate dimensions 0.45 × 0.35 × 0.17 mm was mounted in a thin-walled glass capillary tube in a random orientation on a Nicolet R3m/V automatic diffractometer. Final cell constants, as well as other information pertinent to data collection and refinement, are listed in Table I. The Laue symmetry was determined to be $2/m$, and the space group was shown to be either Cc or $C2/c$. Intensities were measured using the ω-scan technique, with the scan rate depending on the count obtained in rapid prescans of each reflection. Two standard reflections were monitored after every 2 h or every 100 data collected, and these showed no significant decay. In reducing the data, Lorentz and polarization corrections were applied; however, no correction for absorption was made due to the low absorption coefficient.

Since the unitary structure factor statistics were centric and the molecule is capable of lying about a symmetry site, space group $C2/c$ was assumed from the outset. The structure was solved by interpretation of the Patterson map, which revealed the position of two independent Co atoms in the asymmetric unit, which consists of a half-molecule situated on a 2-fold axis passing through the two metals. The remaining nonhydrogen atoms were located in subsequent difference Fourier syntheses. The usual sequence of isotropic and anisotropic refinement was followed, after which all hydrogens were entered in ideal calculated positions and constrained to riding motion, with a single nonvariable isotropic temperature factor. This crystal type is found to contain no excess solvent, which explains its relative hardiness upon removal from the mother liquor. After all shift/esd ratios were less than 0.1, convergence was reached at the agreement factors listed in Table I. No unusually high correlations were noted between any of the variables in the last cycle of full-matrix least-squares refinement, and the final difference density map showed a maximum peak of 0.5 e/Å^3. All calculations were made using Nicolet's SHELXTL PLUS (1987) series of crystallographic programs.

X-ray Data Collection and Processing for $Rh_2(dpb)_4$ and $Rh_2(dpb)_4(CO)$. The same general strategy was used as for the previous compound, with the following differences. For $Rh_2(dpb)_4$: red square plate (0.15 × 0.45 × 0.45 mm), Enraf-Nonius CAD-4, Laue symmetry $4/m$, θ–2θ scan technique, Multan. The asymmetric unit consists of one-quarter of the Rh_2 dimer situated along a 4-fold axis. There is disordered ethanol of crystallization situated near the $\bar{4}$ sites having an approximate population of 0.3 in a general position, thus yielding 1.2 ethanol molecules per dimer. For $Rh_2(dpb)_4(CO)$: burgundy-colored rectangular column (0.15 × 0.20 × 0.35 mm), Enraf-Nonius CAD-4, Laue symmetry $4/mmm$, one-quarter of a molecule per asymmetric unit. Four molecules of disordered water of crystallization were found, each having 50% occupancy.

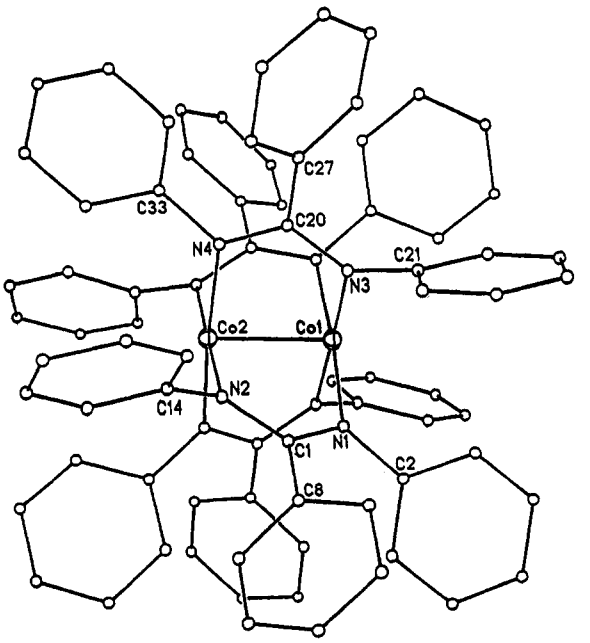

Figure 1. Labeling of key atoms in $Co_2(dpb)_4$. Phenyl atoms are numbered consecutively, beginning at the labeled atom shown.

Results and Discussion

Molecular Structure. The atomic coordinates and selected bond lengths for compounds **1**–**3** are listed in Tables II and III. The molecule $Co_2(dpb)_4$ lies on a 2-fold axis which passes through the two metal atoms (see Figure 1). The Co···Co separation is 2.302 Å, which is slightly longer than the 2.265 Å observed for $Co_2(triaz)_4$[7] but shorter than the Rh–Rh separation of 2.389 Å found in $Rh_2(dpb)_4$.[9] The average Co–N bond distance of 1.942 Å is shorter than the reported Rh–N bond distance of 2.050 Å. The mean N–Co–Co–N torsion angle is 18.4°, which is comparable to 17.0° reported for the triaz analogue[7] and 17.3° found for N–Rh–Rh–N in $Rh_2(dpb)_4$.[9]

The basic differences in the molecular structures of **1** and **2** are those expected from the relative size of the two cations. Because of the shorter Co–Co separation, the two cobalt ions extend slightly more into the equatorial planes of the dpb nitrogens (average Co–Co–N angle = 88.9°) than the two rhodium ions (average Rh–Rh–N angle = 87.4°). The Co–N bond lengths are also shorter. Both of these differences would place a slightly greater steric constraint at the axial sites of **1**.

In our attempt to synthesize the CO adducts of **1** and **2**, we were only able to obtain crystals of $Rh_2(dpb)_4(CO)$ (**3**) suitable for structure determination. Compound **1** shows little tendency toward axial ligation and does not appear to bind CO. The only other CO adducts of dirhodium(II) complexes that have been structurally characterized are $Rh_2(tcl)_4(CO)$ (tcl = thiocaprolactam)[11] and $Rh_2(OOCCH_3)_4(CO)_2$.[12] The molecule $Rh_2(tcl)_4(CO)$ has four sulfur donors and CO bound to one rhodium ion and four amidate nitrogens bound to the second rhodium. In the case of the tetraacetate complex, the CO adduct is not stable and can only be isolated at cold temperatures. The structure shown in Figure 2 and data listed in Table III for $Rh_2(dpb)_4(CO)$ allow us to evaluate the effect of monoligation by the π-acid ligand CO on the molecular structure of a dirhodium(II) complex where the two rhodium(II) centers are in identical equatorial bonding environments.

The Rh–C distance of 1.97 (2) Å falls between the 1.913 (7) and 2.092 Å reported for $Rh_2(tcl)_4(CO)$ and $Rh_2(ac)_4(CO)_2$. The latter complex is a bisadduct, and this accounts in part for the

(11) Lifsey, R. S.; Chavan, M. Y.; Chau, L. K.; Ahsan, M. Q.; Kadish, K. M.; Bear, J. L. *Inorg. Chem.* **1987**, *26*, 822.
(12) Christoph, G. G.; Koh, Y. B. *J. Am. Chem. Soc.* **1979**, *101*, 1422.

Table II. Atomic Coordinates (×10⁴)

$Co_2(dpb)_4$

atom	x	y	z	U(eq),[a] Å²	atom	x	y	z	U(eq),[a] Å²
Co(1)	5000	6343 (1)	2500	31 (1)	C(17)	4222 (3)	1821 (5)	557 (3)	66 (3)
Co(2)	5000	4457 (1)	2500	31 (1)	C(18)	4309 (3)	2874 (5)	396 (3)	63 (3)
N(1)	4170 (2)	6290 (3)	1851 (2)	33 (2)	C(19)	4324 (2)	3747 (5)	767 (2)	45 (3)
N(2)	4322 (2)	4468 (3)	1705 (2)	32 (2)	C(20)	5607 (2)	5417 (5)	1834 (2)	33 (2)
N(3)	5313 (2)	6319 (3)	1884 (2)	35 (2)	C(21)	5168 (2)	7157 (4)	1436 (2)	35 (2)
N(4)	5563 (2)	4514 (4)	2121 (2)	34 (2)	C(22)	5349 (3)	8240 (5)	1603 (3)	61 (3)
C(1)	3971 (2)	5372 (5)	1523 (2)	35 (2)	C(23)	5181 (3)	9056 (5)	1171 (3)	77 (4)
C(2)	3761 (2)	7170 (5)	1796 (2)	38 (2)	C(24)	4848 (3)	8829 (5)	572 (3)	69 (4)
C(3)	3182 (3)	7014 (5)	1767 (2)	52 (3)	C(25)	4664 (3)	7769 (5)	397 (3)	68 (3)
C(4)	2811 (3)	7911 (6)	1727 (3)	70 (3)	C(26)	4827 (2)	6955 (5)	826 (2)	48 (3)
C(5)	3026 (3)	8965 (6)	1750 (3)	75 (4)	C(27)	5965 (2)	5435 (5)	1467 (2)	34 (2)
C(6)	3594 (3)	9129 (5)	1785 (3)	71 (4)	C(28)	6381 (2)	6277 (5)	1547 (2)	41 (2)
C(7)	3970 (3)	8241 (5)	1810 (3)	52 (3)	C(29)	6708 (2)	6310 (5)	1200 (2)	50 (3)
C(8)	3383 (2)	5350 (5)	951 (2)	38 (2)	C(30)	6633 (2)	5513 (6)	773 (2)	52 (3)
C(9)	3244 (2)	6163 (5)	517 (2)	48 (3)	C(31)	6228 (2)	4671 (5)	696 (2)	49 (2)
C(10)	2693 (3)	6136 (5)	−7 (3)	62 (3)	C(32)	5894 (2)	4639 (5)	1037 (2)	43 (2)
C(11)	2282 (3)	5291 (7)	−73 (3)	76 (3)	C(33)	5999 (2)	3658 (5)	2229 (2)	36 (2)
C(12)	2418 (3)	4494 (6)	357 (3)	75 (3)	C(34)	5802 (3)	2583 (4)	2061 (3)	52 (3)
C(13)	2972 (2)	4503 (5)	875 (2)	51 (2)	C(35)	6230 (3)	1730 (5)	2195 (3)	71 (4)
C(14)	4253 (2)	3602 (5)	1297 (2)	38 (2)	C(36)	6836 (3)	1943 (5)	2499 (3)	70 (4)
C(15)	4161 (3)	2529 (5)	1447 (3)	57 (3)	C(37)	7039 (3)	2993 (5)	2667 (3)	61 (3)
C(16)	4149 (3)	1660 (5)	1077 (3)	68 (4)	C(38)	6620 (2)	3849 (4)	2541 (2)	43 (2)

$Rh_2(dpb)_4$

atom	x	y	z	B,[b] Å²	atom	x	y	z	B,[b] Å²
Rh(1)	2500	2500	8497 (9)	2.59 (1)	C(10)	1370 (5)	5927 (5)	10272 (6)	5.4 (2)
Rh(2)	2500	2500	10468 (9)	2.60 (1)	C(11)	1625 (5)	6388 (4)	9447 (7)	5.9 (2)
N(1)	2069 (3)	3594 (3)	8580 (4)	3.0 (1)	C(12)	2068 (4)	6075 (4)	8641 (7)	5.1 (2)
N(2)	2413 (3)	3666 (3)	10398 (4)	2.9 (1)	C(13)	2251 (4)	5307 (4)	8654 (6)	4.1 (2)
C(1)	2163 (3)	4009 (3)	9495 (6)	3.0 (1)	C(14)	2761 (4)	4093 (4)	11262 (5)	3.3 (2)
C(2)	1573 (4)	3836 (4)	7714 (5)	3.4 (2)	C(15)	3377 (4)	4576 (4)	11078 (6)	4.0 (2)
C(3)	1824 (5)	3812 (5)	6617 (6)	4.9 (2)	C(16)	3743 (5)	4916 (5)	11946 (7)	5.6 (2)
C(4)	1360 (5)	3998 (6)	5768 (6)	6.6 (2)	C(17)	3492 (5)	4811 (5)	13015 (7)	6.5 (2)
C(5)	629 (6)	4224 (5)	5989 (7)	7.0 (2)	C(18)	2894 (6)	4328 (6)	13228 (7)	6.5 (2)
C(6)	364 (5)	4263 (5)	7063 (7)	6.0 (2)	C(19)	2513 (5)	3968 (5)	12348 (6)	4.9 (2)
C(7)	826 (4)	4063 (4)	7929 (6)	4.6 (2)	C(20)	7190 (20)	3570 (20)	4890 (30)	7.3 (9)[c]
C(8)	1983 (4)	4850 (4)	9494 (6)	3.3 (1)	C(21)	6530 (30)	3350 (20)	4190 (40)	9.0 (10)[c]
C(9)	1537 (4)	5163 (4)	10308 (6)	4.2 (2)	O(1)	6140 (20)	3070 (20)	4500 (20)	13.4 (9)[c]

$Rh_2(dpb)_4(CO)$

atom	x	y	z	B,[b] Å²	atom	x	y	z	B,[b] Å²
Rh(1)	2500	2500	5670 (1)	2.59 (3)	C(10)	3743 (8)	5924 (7)	4850 (7)	4.9 (4)
Rh(2)	2500	2500	4645 (1)	2.63 (3)	C(11)	3438 (8)	6364 (8)	5265 (6)	4.8 (5)
O(1)	2500	2500	3330 (7)	6.3 (3)	C(12)	2969 (9)	6046 (8)	5651 (6)	4.9 (4)
C(20)	2500	2500	3810 (1)	4.0 (4)	C(13)	2795 (7)	5269 (7)	5628 (5)	3.7 (3)
N(1)	2994 (6)	3567 (6)	5654 (4)	2.4 (2)	C(14)	2352 (7)	4159 (7)	4262 (5)	2.8 (3)
N(2)	2665 (5)	3695 (5)	4717 (3)	2.8 (3)	C(15)	1688 (7)	4543 (7)	4358 (6)	3.7 (4)
C(1)	2936 (7)	3988 (7)	5204 (5)	2.5 (3)	C(16)	1370 (1)	4967 (9)	3939 (6)	5.6 (5)
C(2)	3476 (8)	3811 (7)	6092 (5)	3.1 (3)	C(17)	1730 (1)	5004 (9)	3428 (7)	7.1 (5)
C(3)	3199 (8)	3735 (9)	6633 (5)	4.4 (4)	C(18)	2410 (1)	4617 (8)	3341 (5)	5.9 (4)
C(4)	3630 (7)	3904 (9)	7083 (5)	6.1 (5)	C(19)	2733 (9)	4185 (8)	3751 (5)	4.9 (5)
C(5)	4366 (9)	4154 (9)	6999 (5)	6.7 (5)	O(2)	7710 (10)	970 (10)	2892 (6)	3.8 (4)[c]
C(6)	4658 (9)	4243 (8)	6453 (6)	5.5 (4)	O(3)	6560 (10)	1980 (10)	3255 (8)	6.5 (5)[c]
C(7)	4216 (8)	4037 (9)	6013 (5)	4.9 (4)	O(4)	6870 (10)	1330 (10)	2702 (9)	10.6 (8)[c]
C(8)	3114 (7)	4835 (7)	5203 (5)	2.9 (3)	O(5)	6390 (10)	1640 (10)	2936 (8)	6.2 (6)[c]
C(9)	3579 (8)	5154 (7)	4813 (5)	3.8 (3)					

[a] U(eq) defined as one-third of the trace of the orthogonalized U_{ij} tensor. [b] B defined as $^4/_3[a^2\beta(1,1) + ... + ab(\cos\gamma)\beta(1,2) + ...]$. [c] Atom refined isotropically.

much longer Rh–C bond distance. Ligation by CO results in significant changes in bond distances and bond angles from those of $Rh_2(dpb)_4$. These changes are primarily confined to bonds and angles involving the rhodium ion bound to CO. The Rh–Rh and Rh(2)–N(2) bond distances increase by 0.046 and 0.058 Å whereas the Rh(1)–N(1) bond distance increases only slightly (0.012 Å). Both rhodium ions move toward the bound CO with respect to the bridging ligands upon axial ligation. Rh(2) moves further outside its four-nitrogen equatorial plane by 0.078 Å, and Rh(1) moves into its four-nitrogen plane by 0.055 Å. There is no change in the N–Rh–Rh–N torsional angle.

The large increase in the Rh(2)–N bond distance upon CO ligation shows that there is an increase in electron shielding in the equatorial plane of Rh(2) resulting from the formation of the strong Rh–CO σ bond. In addition to the σ interaction, there should be a considerable π component to the Rh–CO bond due to mixing of the filled π^*_{Rh-Rh} and empty π^*_{CO} molecular orbitals. This interaction will remove π-electron density from the metal centers but will also enhance the σ interaction. The extent of π bonding is more strongly reflected in the CO stretching frequency. For example, the CO stretching frequencies for free CO, $Rh_2(ac)_4(CO)_2$, $Rh_2(dpb)_4(CO)$, and $Rh_2(tcl)_4(CO)$ are 2143, 2108, 2046, and 2025 cm^{-1}, respectively. This is the same trend observed for the Rh–CO bond distances for these complexes.

Spectroscopic Studies on $[Rh_2(dpb)_4]^{0,+}$ and $[Co_2(dpb)_4]^{0,+}$. The visible spectrum of $Rh_2(dpb)_4$ in toluene (Figure S4) consists of

Table III. Selected Bond Lengths (Å)

	$Co_2(dpb)_4$		
Co(1)–N(3)	1.944 (5)	Co(1)–N(1)	1.953 (3)
Co(2)–N(4)	1.943 (5)	Co(2)–N(2)	1.926 (3)
N(1)–C(2)	1.427 (7)	N(1)–C(1)	1.339 (7)
N(2)–C(14)	1.408 (7)	N(2)–C(1)	1.346 (7)
N(3)–C(21)	1.423 (7)	N(3)–C(20)	1.344 (7)
N(4)–C(33)	1.427 (7)	N(4)–C(20)	1.332 (7)
C(20)–C(27)	1.485 (8)	C(1)–C(8)	1.503 (5)
Co(1)–Co(2)	2.302 (1)		
	$Rh_2(dpb)_4$		
Rh(1)–N(1)	2.056 (2)	Rh(2)–N(2)	2.044 (2)
N(1)–C(1)	1.336 (4)	N(1)–C(2)	1.424 (4)
N(2)–C(1)	1.322 (4)	N(2)–C(14)	1.421 (4)
C(1)–C(8)	1.502 (4)	C(2)–C(3)	1.400 (5)
C(8)–C(9)	1.370 (4)	C(14)–C(15)	1.385 (4)
Rh(1)–Rh(2)	2.389 (1)		
	$Rh_2(dpb)_4(CO)$		
Rh(1)–N(1)	2.056 (6)	Rh(2)–N(2)	2.114 (6)
N(1)–C(1)	1.302 (8)	N(1)–C(2)	1.405 (9)
N(2)–C(1)	1.352 (8)	N(2)–C(14)	1.458 (9)
C(1)–C(8)	1.512 (9)	C(2)–C(3)	1.379 (9)
C(8)–C(9)	1.353 (9)	C(14)–C(15)	1.359 (1)
Rh(2)–C(20)	1.97 (2)	C(20)–O(1)	1.151 (14)
Rh(1)–Rh(2)	2.435 (1)		

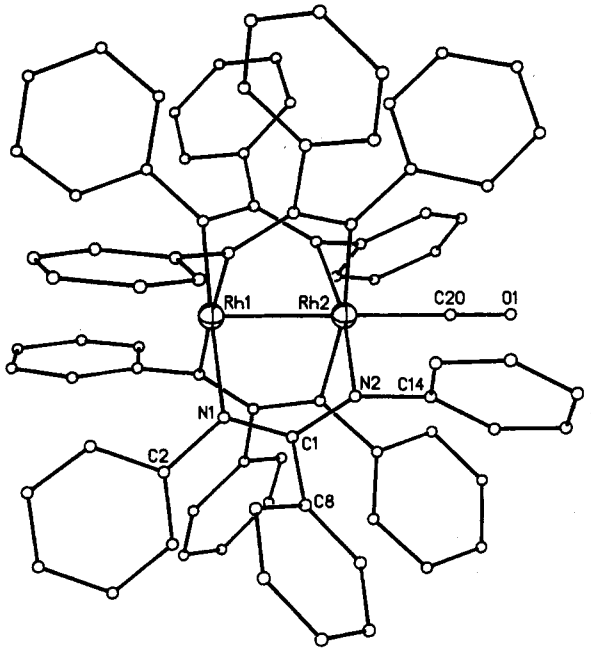

Figure 2. Labeling of key atoms in $Rh_2(dbp)_4(CO)$. Phenyl atoms are numbered consecutively, beginning at the labeled atom shown.

two high-intensity narrow bands at 518 nm ($\epsilon = 6.1 \times 10^3$ M^{-1} cm^{-1}) and 847 nm ($\epsilon = 2.9 \times 10^3$), a weak band at 590 nm ($\epsilon = 3.0 \times 10^2$ M^{-1} cm^{-1}), and a shoulder at 440 nm. The visible bands of **1** (Figure S6a) are slightly higher in energy and have a smaller molar absorptivity than those of **2**. The complex shows two absorption peaks at 485 nm ($\epsilon = 1.6 \times 10^3$) and 718 nm ($\epsilon = 660$). The spectra of the two complexes are invariant in the solvents toluene, dichloromethane, dichloroethane, dimethyl sulfoxide, acetone, pyridine, and tetrahydrofuran. However, in the binding solvent CH_3CN the spectrum of **2** changes significantly. The 518- and 847-nm bands decrease in intensity, and a new broad band at 547 nm of nearly equal intensity appears (Figure S5b). Similar behavior is observed in C_6H_5CN (Figure S5a). The linear –CN group is apparently small enough to extend into the funnellike cavity around the axial sites created by the four *N*-phenyls and bind to rhodium. No change is observed in the spectra of **1** in these solvents. However, the absorbance of $Co_2(dpb)_4$ decreases as a function of time in all the solvents, indicating slow decomposition of the complex. The 518- and 847-nm bands are completely gone from the spectra of $Rh_2(dpb)_4$ in the solvent DMSO containing excess CN^- ($[Rh_2(dpb)_4]/[CN^-] = 0.25$) and CO (1 atm), indicating strong axial bonding by these ligands. Again, no change is observed in the spectrum of **1** in the presence of CN^- or CO.

Table IV. Redox Potentials in Different Solvents

		$E_{1/2}$, V		
compd	solvent	2nd oxidn	1st oxidn	redn
$Co_2(dpb)_4$	CH_2Cl_2	1.45	0.29	−1.64
$Rh_2(dpb)_4$	CH_2Cl_2	1.24	0.23	−1.58
$Co_2(dpb)_4$	CH_3CN	1.25	0.21	−1.53
$Rh_2(dpb)_4$	CH_3CN	1.08	0.05	−1.52
$Co_2(dpb)_4$	DMSO		0.41	−1.44
$Rh_2(dpb)_4$	DMSO		0.34	−1.39
$Co_2(dpb)_4$	THF		0.45	−1.58
$Rh_2(dpb)_4$	THF		0.45	−1.46
$Co_2(dpb)_4$	DMF		0.41	−1.45
$Rh_2(dpb)_4$	DMF		0.32	−1.38

The spectrum of the mixed-valent complex $[Rh_2(dpb)_4Cl]$ in toluene shows two overlapping bands at 445 nm ($\epsilon = 2.4 \times 10^3$) and 520 nm ($\epsilon = 2.5 \times 10^3$) with a shoulder at 650 nm. In addition, a broad, intense near-infrared band is observed at 1030 nm ($\epsilon = 3.6 \times 10^3$) with a shoulder at 830 nm. The intensity and energy of the near-infrared band depend on the nature of the anion. When the axial ligand is CO, CN^-, or CH_3CN, two bands are observed in the near-infrared region. The visible and near-infrared spectrum of the electrochemically generated radical cation complex, $[Co_2(dpb)_4]^+$ (Figure S6b), shows absorption peaks at 1050 nm ($\epsilon = 1180$), 755 nm ($\epsilon = 2990$), 660 nm ($\epsilon = 3650$), and 500 nm ($\epsilon = 7010$). The spectra of $[Co_2(dpb)_4]^+$ and $[Rh_2(dpb)_4]^+$ are similar. However, the peak energies and intensities of $[Co_2(dpb)_4]^+$ are insensitive to the nature of the solvent or the presence of complexing (Cl^-) or nonbinding (ClO_4^-) counterions. This again suggests that $Co_2(dpb)_4$ and $[Co_2(dpb)_4]^+$ show little or no tendency to form axial adducts with neutral or anionic ligands.

Electrochemistry. Redox potentials for **1** and **2** in different solvents and with different axial ligands are listed in Table IV. Two reversible one-electron oxidations and a quasi-reversible one-electron reduction are observed for **2** at $E_{1/2} = 0.23$, 1.24, and −1.58 V vs SCE in CH_2Cl_2.[9] The two oxidation reactions involve the removal of an electron from the HOMO and SOMO, and the reduction involves the addition of an electron to the LUMO.

The cyclic voltammogram of compound **1** (Figure S7b) is almost identical to that reported for compound **2**, in that the same three redox processes are observed. There is a slight anodic shift in the two reversible oxidations for **1** ($E_{1/2} = 0.29$ and 1.45 V vs SCE in CH_2Cl_2, 0.1 M TBAP), whereas the reversible one-electron reduction to form the Co^{I}–Co^{II} complex shows a small cathodic shift ($E_{1/2} = -1.64$ V). The one-electron quasi-reversible reductions of **1** and **2** also occur in the solvents CH_3CN, DMSO, DMF, and THF at potentials cathodically shifted from that found in CH_2Cl_2. The first oxidation potential for $Rh_2(dpb)_4$ shifts anodically under an atmosphere of CO and cathodically in the presence of Cl^-, SCN^-, or CN^-, indicating a stabilization of $[Rh_2(dpb)_4]^+$ by the anionic ligands and a stabilization of $Rh_2(dpb)_4$ by CO.[13] In contrast, no significant change is observed in the first oxidation potential of the dicobalt complex in the presence of the above ligands.

Bulk controlled-potential electrolysis of $Co_2(dpb)_4$ at 0.50 V in CH_2Cl_2, 0.1 M TBAP revealed that one electron per molecule was involved in the first oxidation. The electrolysis at 1.50 V under the same conditions showed a multielectron process for the second oxidation. Apparently, the doubly oxidized complex is only stable at the cyclic voltammetric time scale and decomposes or undergoes a chemical reaction during the time required for bulk electrolysis.

The electrochemistry of **1** and **2** in the presence of CN^- best illustrates the large difference in the propensity of the two complexes for axial ligation. The reversible oxidation of $Rh_2(dpb)_4$

(13) Naris, M. Ph.D. Dissertation, University of Houston, 1986.

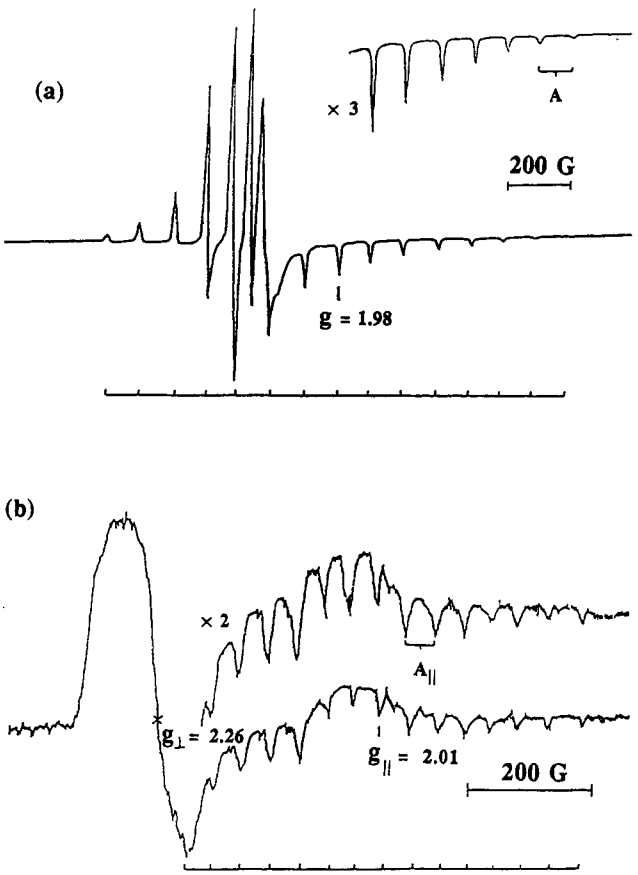

Figure 3. ESR spectra of (a) $[Co^{II}Co^{III}(dpb)_4]^+$ in CH_2Cl_2 and (b) $[Co^{II}Co^{I}(dpb)_4]^-$ in DMF.

at 0.34 V vs SCE in DMSO, 0.1 M TBAP remains reversible and is shifted 570 mV to −0.23 V in the presence of CN^-. This shows that CN^- binds to both $Rh_2(dpb)_4$ and $[Rh_2(dpb)_4]^+$ and strongly stabilizes the $Rh^{II}Rh^{III}$ complex. Completely different electrochemical results are obtained upon the titration of **1** with (TBA)CN, as illustrated by the cyclic voltammograms in Figure S8a–c. As discussed earlier, $Co_2(dpb)_4$ exhibits a reversible oxidation wave at $E_{1/2}$ = 0.29 V with i_{pc}/i_{pa} = 1 (Figure S8a). The potential does not shift in the presence of 2.5 equiv of (TBA)CN, but the anodic current i_{pa} increases while the cathodic current i_{pc} decreases, giving an i_{pc}/i_{pa} of 0.71 (Figure S8b). The addition of 6 equiv of (TBA)CN further decreases i_{pc}/i_{pa} to 0.53 (Figure S8c).

These experimental data indicate that $Co_2(dpb)_4$ does not axially interact with CN^-. However, the oxidation product $[Co_2(dpb)_4]^+$ is reduced back to the neutral complex $Co_2(dpb)_4$ by CN^-, and it is this process that results in the observed decrease in cathodic peak current (i_{pc}) and increase in anodic peak current (i_{pa}) of the cyclic voltammograms. The reduction of $[Co_2(dpb)_4]^+$ by CN^- is further confirmed from UV–visible and ESR spectra. The black solution of the electrochemically generated $[Co_2(dpb)_4]^+$ turned brown upon addition of excess CN^-, and the resulting brown solution gave a UV–visible spectrum identical to that of the neutral complex. In addition, the ESR signal of the radical cation $[Co_2(dpb)_4]^+$ disappeared upon addition of an equivalent amount of CN^-. The solution was reoxidized electrochemically, and the same ESR signal was again observed.

ESR Spectra of $[Co_2(dpb)_4]^+$ and $[Co_2(dpb)_4]^-$. Figure 3a shows the ESR spectrum of a frozen solution (122 K) of $[Co_2(dpb)_4]^+$ generated by controlled-potential electrolysis at +0.50 V in CH_2Cl_2, 0.1 M TBAP. It is clear that the signal at g = 1.98 (g_3) is split into 15 equally spaced lines by the two ^{59}Co ions ($I = {}^7/_2$, 100% natural abundance). The $g_{\perp}$, or possibly a combination of the g_1 and g_2 signals, is complex and overlaps with a portion of the g_3 signal. The splitting in g_3 is consistent with the odd-electron spin density (SOMO) being delocalized on both cobalt ions, as was the case for the corresponding mixed-valent dirhodium complex where a 1:2:1 triplet was observed for $g_{\parallel}$.[9] In addition, g_3 is the same as $g_{\parallel}$ of $[Rh_2(dpb)_4]^+$ ($g_{\parallel}$ = 1.98), for which a δ^*_{Rh-Rh} SOMO has been suggested by theoretical calculations.[14,15] This assignment is not consistent with theoretical calculations[8] on $Co_2(HNNNH)_4$, which gives a σ^* HOMO and a δ^* LUMO. However, the two orbitals were found to be nearly degenerate, and their order could easily, therefore, be inverted. No ESR data are available for other radical cationic complexes containing the $Co^{II}Co^{III}$ unit for comparison. However, the A_3 value of 98.6 × 10^{-4} cm^{-1} is consistent with that of pentacoordinated low-spin Co^{II} cyano complexes reported in the literature.[16,17]

The ESR spectrum of the electrochemically generated $[Co_2(dpb)_4]^-$ is shown in Figure 3b. The complex gives an axial signal with $g_{\perp}$ = 2.26 and $g_{\parallel}$ = 2.01, and the $g_{\parallel}$ is split into 15 equally spaced lines ($A_{\parallel}$ = 39.0 × 10^{-4} cm^{-1}) by the two ^{59}Co ions ($I = {}^7/_2$, 100% natural abundance). Nuclear coupling is also observed in $g_{\perp}$ ($A_{\perp}$ = 16.8 × 10^{-4} cm^{-1}). The ESR spectrum is consistent with a metal-centered reduction with the odd-electron spin density being equally distributed over both cobalt ions. Similar ESR results were reported for the mixed-valent complex $[Rh_2(dpb)_4]^-$. The latter complex also shows an axial signal with $g_{\perp}$ = 2.18 and $g_{\parallel}$ = 2.00 and both $g_{\perp}$ and $g_{\parallel}$ are split into 1:2:1 triplets ($A_{\perp}$ = 9.0 × 10^{-4} cm^{-1}, $A_{\parallel}$ = 16.0 × 10^{-4} cm^{-1}) by the two ^{103}Rh ions ($I = {}^1/_2$, 100% natural abundance). The ESR results are consistent with a σ^*_{Rh-Rh} and a σ^*_{Co-Co} SOMO for the two complexes.[14,15]

In summary, the successful synthesis of the complex $Co_2(dpb)_4$ allows the first direct comparison of the isoelectronic $Co_2^{5+,4+,3+}$ and $Rh_2^{5+,4+,3+}$ dimer units in an identical equatorial ligand environment. Compounds **1** and **2** have the same basic molecular structure. The propensity for Co(II)–Co(II) bond formation increases when the two cobalt(II) ions are bound to strongly basic anionic nitrogen donor ligands. This is illustrated by the short Co–Co separations of 2.265 and 2.302 Å found for $Co_2(triaz)_4$[3] and $Co_2(dpb)_4$, respectively, and the long Co–Co bond distance (2.832 Å) found for $Co_2(OOCPh)_4$(quinoline). For dirhodium complexes, the substitution of dpb for carboxylate bridging ligands has very little effect on the Rh–Rh separation. However, the metal-centered orbitals are raised in energy by approximately 1 V as a result of nitrogen donor for oxygen donor atom substitution.[18] Therefore, the 3d orbitals of $Co_2(dpb)_4$ should also be considerably higher in energy than the corresponding orbitals of the carboxylate complex. This charging effect should make the Co(II) 3d orbitals more diffuse and overlap with each other more; consequently, this could account for the stronger Co(II)–C(II) bond in $Co_2(dpb)_4$. The formation of a strong Co–Co bond appears to decrease the tendency of the cobalt centers to form even one axial ligand bond as is the case for $Co_2(OOCPh)_4$(quinoline). It is well documented that low-spin cobalt(II) (strong ligand field) complexes tend to form four- and five-coordinate complexes as a result of a Jahn–Teller distortion, and this may be the case here. The visible spectra, redox reactions, and ESR spectra of the dicobalt and dirhodium complexes studied are similar. However, there are major differences in the chemical reactivities of **1** and **2** with respect to axial ligation. Both $[Rh_2(dpb)_4]^-$ and $[Co_2(dpb)_4]^-$ are unique, highly reactive radical-anion complexes and offer interesting molecules for future chemical studies.

Acknowledgment. The support of the Robert A. Welch Foundation (Grant No. E-918) is gratefully acknowledged.

Registry No. $Co_2(dpb)_4$, 138259-87-7; $Co(C_{10}H_{17}O_2)_2$, 38582-17-1; $Rh_2(dpb)_4$, 138259-88-8; $Rh_2(dpb)_4(CO)$, 138259-89-9; $[Rh_2(dpb)_4Cl]$, 138259-90-2; $[Co_2(dpb)_4]^+$, 138259-91-3; CN^-, 57-12-5; $[Co_2(dpb)_4]^-$,

(14) Kawamura, T.; Katayama, H.; Yamabe, T. *Chem. Phys. Lett.* **1986**, *130*, 20.
(15) Kawamura, T.; Fukamachi, K.; Sowa, T.; Hayashida, S.; Yonezawa, T. *J. Am. Chem. Soc.* **1981**, *103*, 364.
(16) Alexander, J. J.; Gray, H. B. *J. Am. Chem. Soc.* **1967**, *89*, 3356.
(17) Taylor, R. J.; Drago, R. S.; George, J. E. *J. Am. Chem. Soc.* **1989**, *111*, 6610.
(18) Ahsan, M. Q.; Bernal, I.; Bear, J. L. *Inorg. Chem.* **1986**, *25*, 260.

138259-92-4; $[Rh_2(dpb)_4]^+$, 99148-27-3; $[Rh_2(dpb)_4]^{2+}$, 99165-18-1; $[Co_2(dpb)_4]^{2+}$, 138259-93-5; Co, 7440-48-4; Rh, 7440-16-6.

Supplementary Material Available: For **1-3**, Tables SI-SIV, listing data collection and processing parameters, hydrogen atomic coordinates, complete bonding geometry, and anisotropic thermal parameters, and Figures S1-S8, showing packing diagrams, visible and near-IR spectra, and cyclic voltammograms (22 pages); tables of observed and calculated structure factors (35 pages). Ordering information is given on any current masthead page.

Contribution from the Laboratoire de Chimie Inorganique, URA No. 420, Université de Paris-Sud, 91405 Orsay, France, Laboratoire de Chimie des Métaux de Transition, URA No. 419, 75232 Paris, France, and Service National des Champ Intenses, UPR No. 5021, 38042 Grenoble, France

Weak Ferromagnetism in the Molecular Compound Cu(ta)(3-pic)·H_2O (ta = Terephthalato, 3-pic = 3-Picoline). Crystal Structure of Cu(ta)$(3\text{-pic})_2$·0.5(3-pic)·0.5CH_3OH

Evangelos Bakalbassis,[1a] Pierre Bergerat,[1a] Olivier Kahn,*[,1a] Suzanne Jeannin,[1b] Yves Jeannin,[1b] Yves Dromzee,[1b] and Maurice Guillot[1c]

Received May 29, 1991

The two compounds Cu(ta)$(3\text{-pic})_2$·0.5(3-pic)·0.5CH_3OH (**1**) and Cu(ta)(3-pic)·H_2O (**2**) have been synthesized, ta standing for terephthalato and 3-pic for 3-picoline. The crystal structure of **1** has been determined. **1** crystallizes in the monoclinic system, space group $P2_1/c$, with $a = 9.703$ (4) Å, $b = 13.184$ (8) Å, $c = 19.825$ (4) Å, $\beta = 115.12$ (2)°, and $Z = 4$. The structure consists of Cu(ta) infinite layers, to which the 3-pic molecules are perpendicular, and noncoordinated 3-pic and CH_3OH molecules. In the lattice the Cu(ta)$(3\text{-pic})_2$ units are centrosymmetrically related, affording copper(II) pairs with a Cu···Cu separation of 4.414 Å. Those pairs are linked together through terephthalate bridges. **1** spontaneously evolves in air to yield **2**. The copper(II) ions in **1** are magnetically isolated. In contrast, the magnetic properties of **2** are quite unusual. Magnetic susceptibility measurements together with EPR spectra and low-field (5 G) and high-field (up to 20 T) magnetization data lead to the following description: **2** consists of antiferromagnetically coupled copper(II) pairs with a singlet-triplet energy gap $J \approx -330$ cm^{-1}. In addition, antisymmetric interaction gives rise to a residual magnetic moment in the ground state. The pairs weakly couple through the terephthalate bridges in such a way that the pair magnetic moments align along the same direction. **2** exhibits a weak ferromagnetic transition at $T_c = 2.8$ K.

Introduction

More and more researchers working with open-shell molecules are interested by the bulk magnetic properties.[2] One of the main challenges in this field is then to design molecular-based compounds exhibiting a spontaneous magnetization. Spectacular results along this line have recently been reported.[3-14] Additionally, molecules with a high-spin multiplicity in the ground state have been described.[15-18]

To design molecular materials displaying a zero-field magnetization below a critical temperature T_c, one must assemble magnetic molecular units in such a way that the interaction between the local spin carriers at the scale of the lattice leads to a nonzero resulting spin. This result can be achieved under various conditions as follows: (i) All the interactions between nearest neighbors are ferromagnetic. If so, the local spins tend to align along the same direction and a ferromagnetic transition is expected to occur at a critical temperature T_c. (ii) All the interactions between nearest neighbors are antiferromagnetic, but owing to a noncompensation of the interacting local spins, the resulting spin is different from zero. If intra- and intermolecular interactions are not distinguished, this system is called a ferrimagnet and a magnetically ordered state with a spontaneous magnetization is again expected below the critical temperature T_c. (iii) All the spin carriers are similar and couple antiferromagnetically, with nevertheless a small canting, so that there is a nonzero resulting spin. If so, a weak ferromagnetic transition is expected at T_c. (iv) Finally, a nonzero resulting spin may arise from very complicated

(1) (a) Université de Paris-Sud. (b) URA No. 419. (c) UPR No. 5021.
(2) Gatteschi, D., Kahn, O., Miller, J., Palacio, F., Eds. *Molecular Magnetic Materials*; NATO ASI Series; Klüwer: Dordrecht, The Netherlands, 1991.
(3) Miller, J. S.; Calabrese, J. C.; Rommelmann, H.; Chittipeddi, S. R.; Zhang, J. H.; Reiff, W. M.; Epstein, A. J. *J. Am. Chem. Soc.* **1987**, *109*, 769.
(4) Miller, J. S.; Epstein, A. J.; Reiff, W. M. *Science* **1988**, *240*, 40; *Chem. Rev.* **1988**, *88*, 201; *Acc. Chem. Res.* **1988**, *21*, 114.
(5) Broderick, W. E.; Thomson, J. A.; Day, E. P.; Hoffman, B. M. *Science* **1990**, *249*, 401.
(6) Kahn, O.; Pei, Y.; Verdaguer, M.; Renard, J. P.; Sletten, J. *J. Am. Chem. Soc.* **1988**, *110*, 782.
(7) Nakatani, K.; Carriat, J. Y.; Journaux, Y.; Kahn, O.; Lloret, F.; Renard, J. P.; Pei, Y.; Sletten, J.; Verdaguer, M. *J. Am. Chem. Soc.* **1989**, *111*, 5739.
(8) Nakatani, K.; Bergerat, P.; Codjovi, E.; Mathonière, C.; Pei, Y.; Kahn, O. *Inorg. Chem.* **1991**, *30*, 3977.
(9) Pei, Y.; Kahn, O.; Nakatani, K.; Codjovi, E.; Mathonière, C.; Sletten, J. *J. Am. Chem. Soc.* **1991**, *113*, 6558.
(10) Caneschi, A.; Gatteschi, D.; Renard, J. P.; Rey, P.; Sessoli, R. *Inorg. Chem.* **1988**, *27*, 1756.
(11) Caneschi, A.; Gatteschi, D.; Sessoli, R.; Rey, P. *Acc. Chem. Res.* **1989**, *22*, 392.
(12) Caneschi, A.; Gatteschi, D.; Renard, J. P.; Rey, P.; Sessoli, R. *Inorg. Chem.* **1989**, *28*, 1676; **1989**, *28*, 2940.
(13) Zhong, Z. J.; Matsumoto, N.; Okawa, H.; Kida, S. *Chem. Lett.* **1990**, 87.
(14) Matsumoto, N.; Sakamoto, M.; Tamaki, H.; Okawa, H.; Kida, S. *Chem. Lett.* **1990**, 853.
(15) Iwamura, H. *Adv. Phys. Org. Chem.* **1990**, *26*, 179.
(16) Fujita, I.; Teki, Y.; Takui, T.; Kinoshita, T.; Itoh, K.; Miko, F.; Sewaki, Y.; Iwamura, H.; Izuoka, A.; Sagawara, T. *J. Am. Chem. Soc.* **1990**, *112*, 4074.
(17) Caneschi, A.; Gatteschi, D.; Laugier, J.; Rey, P.; Sessoli, R.; Zanchini, C. *J. Am. Chem. Soc.* **1988**, *110*, 2795.
(18) Boyd, P. D. W.; Li, Q.; Vincent, J. B.; Folting, K.; Chang, H. R.; Streib, W. E.; Huffman, J. C.; Christou, G.; Hendrickson, D. N. *J. Am. Chem. Soc.* **1988**, *110*, 8537.

0020-1669/92/1331-0625$03.00/0